



Turning the unwanted surface bismuth enrichment to favourable BiVO₄/BiOCl heterojunction for enhanced photoelectrochemical performance

Cong Liu, Jinglan Zhou, Jinzhan Su*, Liejin Guo*

International Research Center for Renewable Energy, State Key Laboratory of Multiphase Flow in Power Engineering, Xi'an Jiaotong University, Shaanxi, 710049, PR China



ARTICLE INFO

Keywords:

Bismuth enrichment
BiVO₄/BiOCl heterojunction
Water oxidation

ABSTRACT

Bismuth enrichment as a common issue at the surface of bismuth vanadate (BiVO₄) has been frequently reported as a severe limitation to its water oxidation kinetics. To address this problem, this study reports a novel approach to eliminate the surface bismuth enrichment by forming BiVO₄/BiOCl heterojunction via surface hydrochloric acid treatment. Benefiting from type II band alignment of the BiVO₄/BiOCl heterojunction, the treated photoanode delivers excellent PEC performance with a photocurrent density of 1.83 mA/cm² at 1.23 V (vs. Ag/AgCl), compared to 1.27 mA/cm² of untreated BiVO₄ photoanode. This improvement could be attributed to the effective charge separation in heterojunction interface as the charge separation efficiency of BiVO₄ increased from 28% to 41% at 1.23 V (vs. Ag/AgCl) after formation of BiVO₄/BiOCl heterojunction.

1. Introduction

Over the past decades, the utilization of semiconductor photoanodes for sunlight-assisted hydrogen production has gained considerable momentum, due to the increasing concern on energy issues [1–3]. Monoclinic bismuth vanadate (BiVO₄) as one of potential photoanode materials has been widely reported for photoelectrochemical (PEC) water oxidation [4–7]. The outstanding merits of BiVO₄ are wide light absorption range (bandgap of 2.4 eV), appropriate band edge positions (0.2 and 2.6 eV vs. RHE for conduction band and valence band, respectively) and high photocorrosion resistance (stable at pH = 3–11) [8–10]. However, the PEC activity of BiVO₄ is still limited by a number of factors, such as short holes diffusion length, excessive charge recombination, poor charge transport properties, and slow water oxidation kinetics [11–13]. To address these limitations, various strategies have been developed to improve the PEC prosperities of BiVO₄ photoanodes, including metal doping (Mo [14], W [15]) to enhance its donor density and holes diffusion length, integration of heterojunctions (WO₃/BiVO₄ [16–18], TiO₂/BiVO₄ [19]) or homo-junctions [20] to expedite the charge separation of photoinduced carriers, fabrication of novel nanostructures (nanoporous [21], nanopillar [22]) to improve its charge transport properties as well as decoration of co-catalysts (CoO_x [23,24], CoPi [25]) to facilitate the oxygen evolution reaction (OER).

Recently, Choi's group [21] has fabricated BiVO₄ photoanodes with a high photocurrent ($1.8 \pm 0.3 \text{ mA/cm}^2$ at 1.23 V vs. RHE) via

changing of BiOI to BiVO₄ in the presence of vanadylacetetylacetone (VO(acac)₂). Inspired by this approach, a multi-step ion exchange approach was used to prepare porous BiVO₄ photoanodes in our lab [26]. Both approaches contain one same step, which is removing of excess V₂O₅ by soaking BiVO₄ photoanodes in NaOH solution. To confirm the effect of soaking in NaOH solution on the surface composition of BiVO₄ photoanode, we performed the XPS measurement for the treated BiVO₄ photoanode. The XPS results show that NaOH treatment reduced amount of V element in the BiVO₄ surface part (Fig. S1 and Table S1), resulting in surface bismuth enrichment. However, the bismuth enrichment is detrimental to its photocurrent response. Rossell and his group [27] revealed that the bismuth enrichment would raise the Fermi level of BiVO₄ at the surface part and result in the formation of type II homojunction. Wang and his group [28] reported that the excessive reduction of V⁵⁺ to V⁴⁺ would create much oxygen vacancies, which are detrimental to the PEC performance of BiVO₄. This is because the V⁴⁺ with large radius acts as scattering centers and reduces the diffusion length of holes. In this regard, there is a significant to pursue a solution to avoiding bismuth enrichment in the BiVO₄ surface part.

Integration with surface heterojunction is one of promising methods to adjust the surface properties of BiVO₄, such as surface charge separation and surface kinetics [29,30]. Many BiVO₄ based n-p type heterojunction photoanodes were reported for PEC water oxidation, like BiVO₄/BiOI [31], BiVO₄/ZnFe₂O₄ [32] and BiVO₄/CaFe₂O₄ [29] heterojunction photoanodes. All these n-p type heterojunctions showed

* Corresponding authors.

E-mail addresses: j.su@mail.xjtu.edu.cn (J. Su), lj-guo@mail.xjtu.edu.cn (L. Guo).

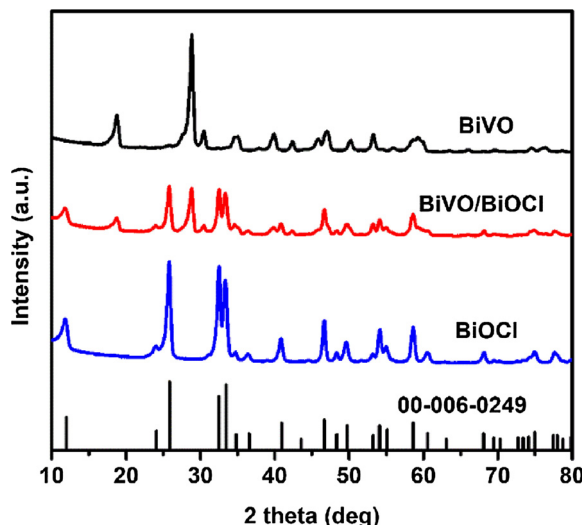


Fig. 1. XRD patterns of BiVO, BiVO/BiOCl and BiOCl samples.

enhanced PEC performances due to their formed type II heterojunction. Similar to the reported BiOI semiconductor, BiOCl as a p-type semiconductor [33] is also a good candidate for fabricating BiVO₄ based heterojunction for PEC water oxidation because the band edge difference between these two materials is large enough to provide a strong electric field for separation of photo-induced carriers under illumination [34,35]. However, to the best of our knowledge, there is no report on BiVO₄/BiOCl heterojunction photoanodes for water oxidation except for a few studies on photocatalyst for pollutant degradation, such as methyl orange [36], methylene blue [37], rhodamine B [38] and photosensitization [39] degradations. Furthermore, most of the methods for preparing BiVO₄/BiOCl photocatalyst are directly synthesis of both components simultaneously, which are easy to form undesired defects at the heterojunction interfaces. Thus, the lack of fabricating approach for BiVO₄/BiOCl heterojunction leaves an important gap in the adjusting of BiVO₄ surface properties and using of BiVO₄/BiOCl heterojunction for PEC water oxidation.

Herein, we report a simple method to turn the unwanted bismuth

Table 1

Surface elemental atomic compositions of BiVO, BiVO/BiOCl and BiOCl samples by EDS.

	Bi (%)	V (%)	O (%)	Cl (%)
BiVO	19.87	16.44	63.67	0.02
BiVO/BiOCl	25.65	9.85	51.09	13.41
BiOCl	30.51	0.40	42.31	26.78

enrichment to favourable BiVO₄/BiOCl heterojunctions via a direct replacement of V⁵⁺ ions by Cl⁻ ions through soaking BiVO₄ photoanodes in diluted HCl solution. The BiVO₄ photoanodes (BiVO) used were prepared by our previously reported multistep ion exchange approach [26]. The fabrication of optimal BiVO/BiOCl heterojunction was achieved by immersing BiVO in 75 mM hydrochloric acid (HCl) solutions for 24 h, while using a 150 mM hydrochloric acid (HCl) solution resulted in fully conversion of BiVO₄ to BiOCl. This method effectively avoids the bad influences of bismuth enrichment in the surface part of BiVO₄ as well as forming a BiVO₄/BiOCl heterojunction with a type II band alignment, which boosts the PEC water oxidation performance of obtained photoanode.

2. Experimental

2.1. Preparation of photoanodes

Vanadyl acetylacetone (VO(acac)₂) was purchased from Sigma Aldrich. All other chemicals were purchased from Sinopharm Chemical Reagent Co., Ltd. (China) without further purification. All aqueous solutions were prepared using de-ionized water (resistivity $\geq 18.2 \text{ M}\Omega \text{ cm}$, Ulupure: UPD-II-20 T, China). Fluorine-doped tin oxide (FTO, 8Ω/□) substrates were purchased from Nippon Sheet Glass (NSG) group.

Preparation of BiVO sample: BiVO sample was prepared by our previously reported multistep ion exchange approach [26]. The difference from previous approach is that NH₄VO₃ dissolved in H₂O as vanadium resource in this experiment instead of vanadyl acetylacetone (VO(acac)₂) dissolved in dimethyl sulfoxide (DMSO) solution as the unbearable burning smell of DMSO. The detail process as shown in

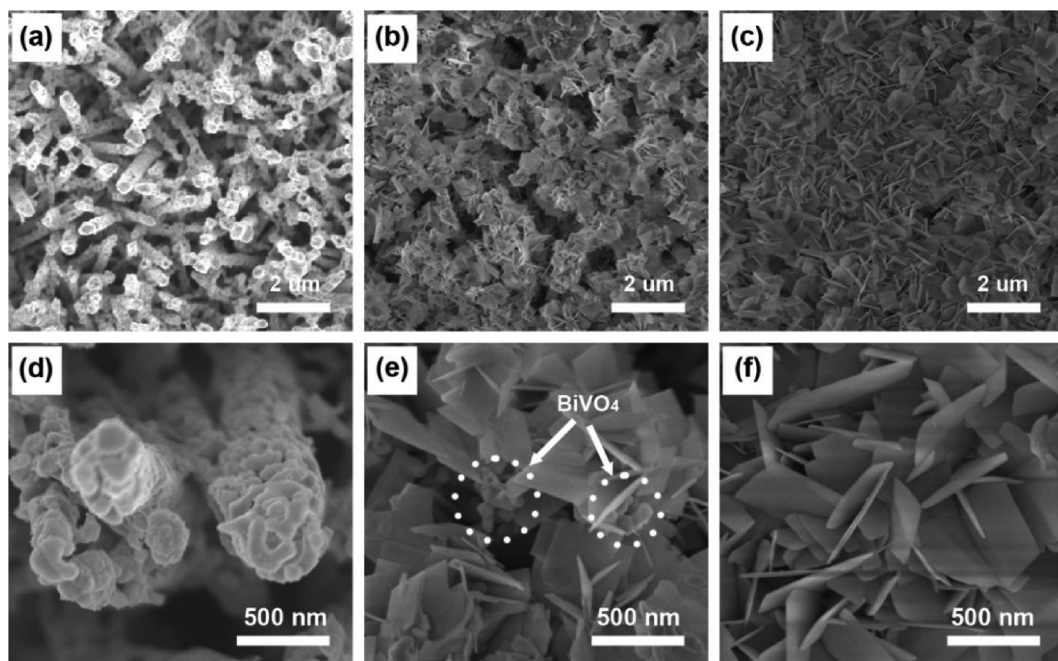


Fig. 2. SEM images of (a, d) BiVO, (b, e) BiVO/BiOCl and (c, f) BiOCl samples.

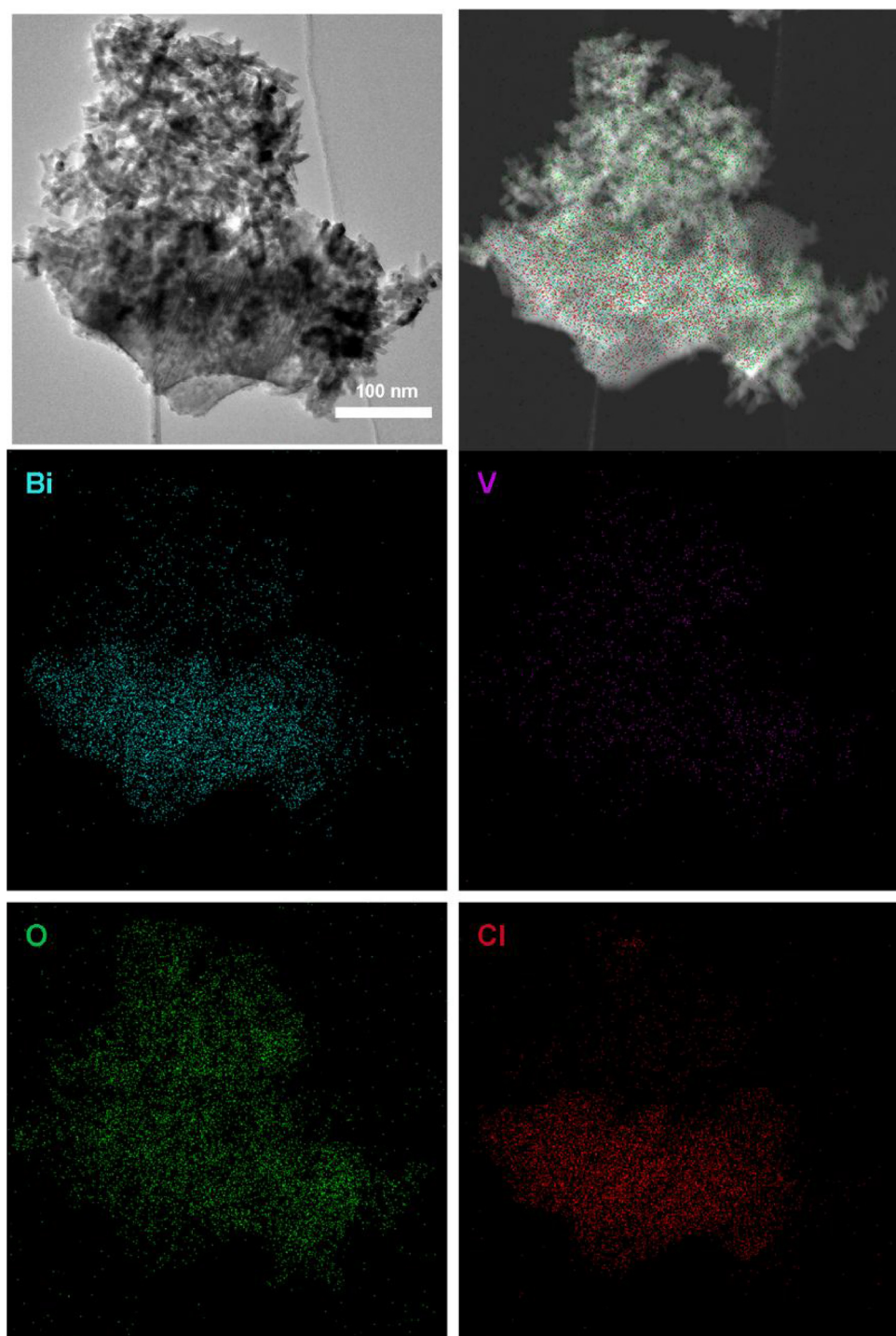


Fig. 3. TEM and corresponding elemental mapping images of BiVO/BiOCl sample.

supporting information.

Preparation of BiVO/BiOCl sample: As-prepared BiVO sample was immersed in 75 mM hydrochloric acid (HCl) solutions for 24 h, resulted in BiVO/BiOCl sample.

Preparation of BiOCl sample: As-prepared BiVO sample was immersed in 150 mM hydrochloric acid (HCl) solutions for 24 h, resulted in BiOCl sample.

2.2. Characterization of photoanodes

X-ray diffraction (XRD, PANalytical X'pert MPD Pro Diffractometer)

was used to determine the crystallinity of the samples. Field emission scanning electron microscopy (FE-SEM, JEOL JSM-7800FE) equipped with an energy dispersive X-ray spectrometer (EDS) was used to study the morphologies and surface elemental compositions of the samples. Transmission electron microscopy (TEM) with an energy dispersive X-ray spectrometer (EDS) elemental mapping was used to confirm the surface elemental distributions of the samples. X-ray photoelectron spectroscopy (XPS, Axis UltraDLD, Kratos) with a monochromated Al K α line as the X-ray source was used to reveal the surface chemical compositions of the samples and the binding energies were calibrated with respect to the residual C 1 s peak at 284.8 eV. UV-vis

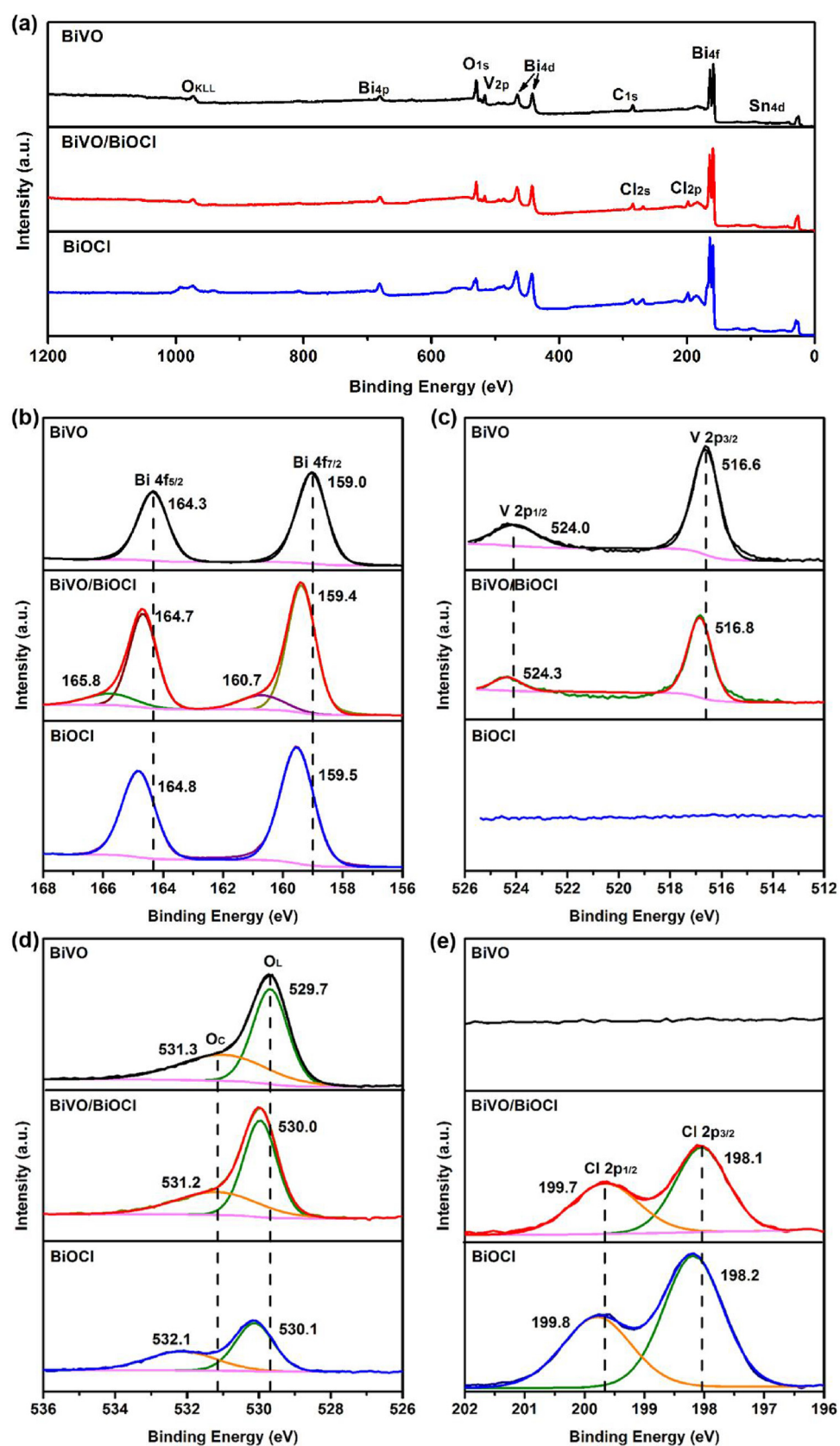


Fig. 4. XPS spectrum of the three samples for (a) Bi 4f, (b) V 2p, (c) O 1s and (d) Cl 2p.

Table 2

Surface elemental atomic compositions of BiVO_x, BiVO/BiOCl and BiOCl samples by XPS.

	Bi (%)	V (%)	O (%)	Cl (%)
BiVO	19.76	11.77	68.48	0.00
BiVO/BiOCl	26.16	5.83	54.44	13.57
BiOCl	30.43	0.00	42.11	27.45

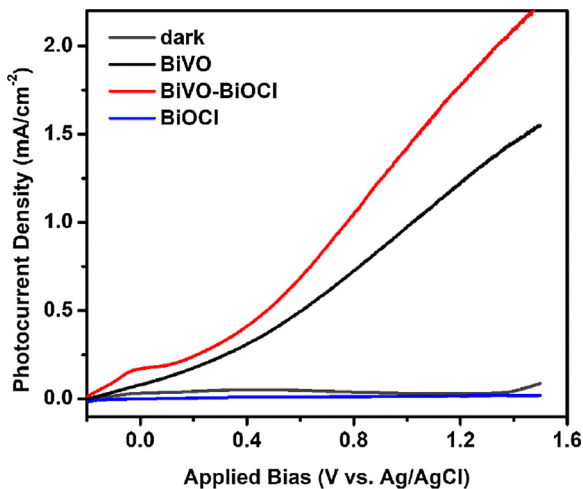


Fig. 5. Photocurrent density versus applied bias curves for the samples of BiVO, BiVO/BiOCl and BiOCl, recorded in 0.5 M Na₂SO₄ solution.

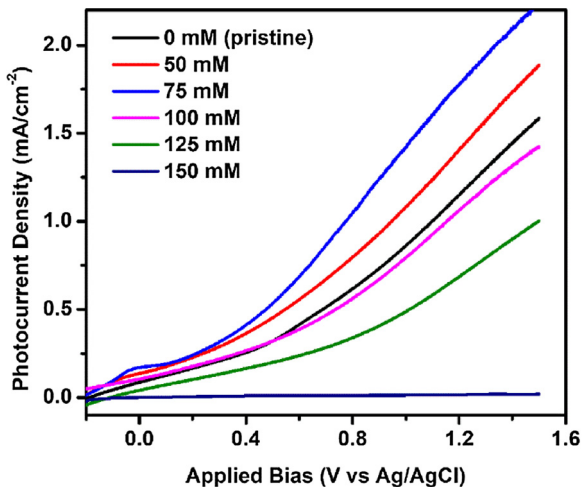


Fig. 6. Linear sweep voltammograms for BiVO₄ samples treated with HCl at various concentrations, recorded in 0.5 M Na₂SO₄ solution.

spectrophotometer (Hitachi U-4100) was used to record the Uv-vis spectrum of the samples. Ultraviolet photoelectron spectroscopy (UPS) was used to detect the valance band (VB) level of the samples.

2.3. Photoelectrochemical (PEC) measurements

PEC results were recorded with an electrochemical workstation of CHI 760D. The PEC measurements were performed in 0.5 M Na₂SO₄ solution by using a conventional three-electrode cell configuration, with the samples as the working electrodes, an Ag/AgCl reference electrode, and a Pt plate as the counter electrode. The light source used in the PEC measurements was a 300 W xenon lamp with an AM 1.5 G filter (with an illumination intensity of 100 mW·cm⁻²), and the samples were illuminated from the backside with an area of 0.785 cm² (circular

diameter = 1 cm).

3. Discussion and results

3.1. Structural characterization of BiVO, BiVO/BiOCl and BiOCl samples

XRD was used to characterize the phase and crystallinity of as-prepared samples, with the results shown in Fig. 1. The diffraction peaks of BiVO and BiOCl samples were assigned to monoclinic BiVO₄ (JCPDS: 00-14-0688) and tetragonal BiOCl ((JCPDS: 00-06-0249), respectively. The coexistence of BiVO₄ and BiOCl phases without any impurity peaks in BiVO/BiOCl sample indicates the successfully synthesis of BiVO/BiOCl heterojunction.

Scanning electron microscope (SEM) equipped with an energy dispersive X-ray spectrometer (EDS) was used to investigate their morphology (Fig. 2) and surface elemental composition (Table 1). The top-viewed SEM images shown in Fig. 2(a, d) and (c, f) illustrate the porous nanorods structure of BiVO sample and nanosheets structure of BiOCl samples, respectively. While in Fig. 2(b, e), a morphology of BiVO₄ nanorods covered with BiOCl nanosheets was observed for the BiVO/BiOCl sample. By analysis of surface elemental compositions of the samples (Table 1), one can find that unwanted Bi enrichment was observed for BiVO sample. After surface hydrochloric acid treatment, the content of V element decreased to 9.85%, Cl element increased to 13.41% for BiVO/BiOCl sample, indicates the formation of BiVO/BiOCl heterojunction. Further treatment with 150 mM HCl, 0.40% V and 26.78% Cl were observed for BiOCl sample, indicates the complete replacement of V by Cl.

Transmission electron microscopy (TEM) mapping was used to characterize the element distribution of Bi, V, O and Cl on BiVO/BiOCl sample to further confirm the successfully synthesis of BiVO/BiOCl heterojunction, as shown in Fig. 3. The main compositions of the scattered nanorods are Bi, V and O elements, indicates the porous nanorods corresponding to BiVO₄. The main compositions of the nanosheets are Bi, O and Cl elements, indicates the nanosheets corresponding to BiOCl.

3.2. Formation mechanism of BiOCl in the BiVO/BiOCl heterojunction

X-ray photoelectron spectroscopy (XPS) was used to track the change of surface chemical composition [28] before and after the formation of BiOCl by surface hydrochloric acid treatment, as shown in Fig. 4 and Table 2. Fig. 4 shows the XPS spectrum of the three samples of BiVO, BiVO/BiOCl and BiOCl. Before surface HCl treatment, the main elemental components of BiVO are Bi, V and O. After 75 mM HCl treatment, a new elemental component of Cl appeared. Interestingly, a shoulder was found for both Bi 4f_{5/2} and Bi 4f_{7/2} envelope on the high binding energy side (Fig. 4b). Two different peaks can be observed by fitting of these envelopes, which suggested the existence of two different Bi atoms corresponding to BiVO₄ and BiOCl in the BiVO/BiOCl heterojunction. For the sample BiOCl treated with 150 mM HCl, the peak for V disappeared, indicating the complete transform of BiVO₄ to BiOCl.

For a metal atom, the XPS binding energy is proportional to the density of outer electrons [14]. Usually, anion atom (e.g. oxygen) is much more electrophilic than metal atom, so the metal-anion (e.g. metal-O) bond formed by outer electron transfer from the metal atom to anion atom. (1) If the anion replaced by another with higher electrophilicity, the outer electron density of the metal atom will decrease, resulting in decrease of XPS binding energy. (2) If the anion replaced by one with lower electrophilicity, the outer electron density on metal atom will increase and its XPS binding energy increases. Fig. 4b shows typical XPS Bi 4f core states of these three samples. Two binding energies of BiVO were observed at 159.0 and 164.3 eV corresponding to the Bi 4f_{7/2} and Bi 4f_{5/2}, respectively. By comparison, these peaks shifted to higher level after surface HCl treatment, indicating that the Bi-O bonds

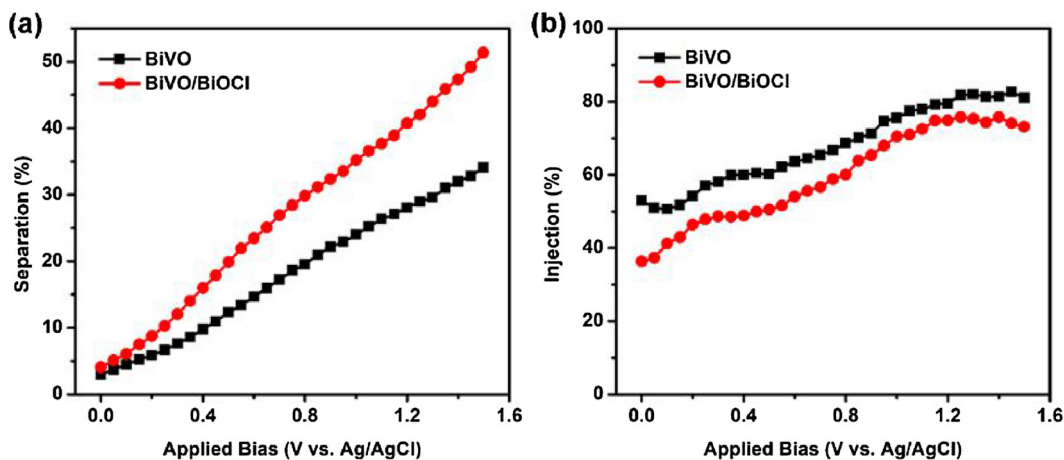


Fig. 7. (a) Charge separation and (b) injection efficiencies of BiVO and BiVO/BiOCl samples.

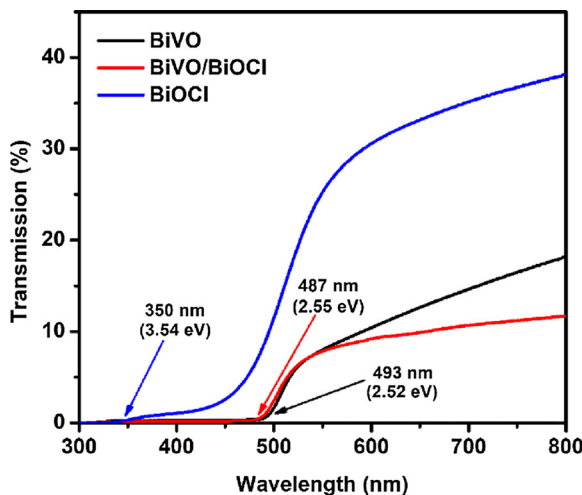


Fig. 8. UV-vis diffuse transmission spectra (DRS) of BiVO, BiVO/BiOCl and BiOCl samples.

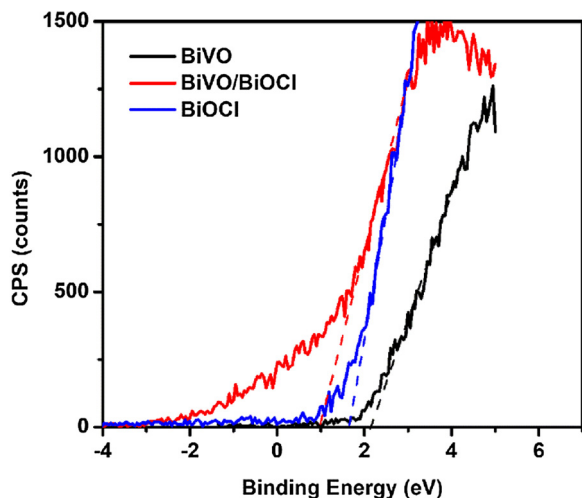


Fig. 9. UPS results of BiVO, BiVO/BiOCl and BiOCl samples.

in BiVO_4 crystal on BiVO/BiOCl and BiOCl samples both cracked [14]. Fig. 4c presents the V 2p XPS results of the three as-prepared samples. For the BiVO sample, the binding energy peaks of V $2\text{p}_{3/2}$ and V $2\text{p}_{5/2}$ locate at 516.6 and 524.0 eV, respectively. Similarly, these peaks shifted to higher level after surface HCl treatment, indicating that the

V–O bonds in BiVO/BiOCl heterojunction also cracked. Fig. 4d shows the XPS peaks of O 1s. For the sample of BiVO, it is shown that the O 1s core can be split into two peaks, 529.7 and 531.3 eV, which represent the lattice oxygen and chemically adsorbed oxygen [19], respectively. The peaks shifted to the higher energy direction after surface HCl treatment, meaning the state of metal–oxygen bonds in the sample BiVO/BiOCl and BiOCl crystals were changed. It is noted that both cracking of Bi–O and V–O bonds cannot increase the outer electron density of oxygen atom. By considering the formation of BiOCl (Figs. 1–3), one can conclude the O–Cl covalent bond was formed after surface HCl treatment. The XPS result of Cl 2p is shown in Fig. 4e. No peak was observed in the BiVO sample. For the BiVO/BiOCl sample, two peaks for the Cl 2p at 198.1 and 199.7 eV are observed, which can be assigned to Cl $2\text{p}_{3/2}$ and Cl $2\text{p}_{1/2}$, respectively. The full conversion of O–V bond to O–Cl covalent bond results in blue shift of Cl 2p peaks after further surface treatment for the sample of BiOCl. Furthermore, one can extract the surface elemental atomic compositions of the three samples based on the XPS integral (Table 2) and summarize a same result corresponding to EDS.

Based on above discussion, the BiOCl formation mechanism is depicted as follows. At the BiVO_4 surface, Cl atoms attack Bi and V atoms, resulting in cracking of Bi–O and V–O bonds, respectively. The formation of O–Cl covalent bonds are easier to connect with Bi than V atoms as the electrophilic of Bi better than V according to Pauling and Allen scales, resulting in V atoms releasing from BiVO_4 in an acidic environment and BiVO_4 converting to BiOCl eventually.

3.3. PEC performance of BiVO, BiVO/BiOCl and BiOCl samples

Fig. 5 displays photocurrent density versus potential curves recorded under the dark and AM 1.5 G simulated sunlight illumination ($100 \text{ mW} \cdot \text{cm}^{-2}$). It can be seen that the sample of BiVO shows a photocurrent density of $1.27 \text{ mA} \cdot \text{cm}^{-2}$ at 1.23 V (vs. Ag/AgCl). By introducing a heterojunction of BiVO/BiOCl, a much better photocurrent density of $1.83 \text{ mA} \cdot \text{cm}^{-2}$ at 1.23 V (vs. Ag/AgCl) is achieved for the sample of BiVO/BiOCl. The complete conversion of BiOCl shows a photocurrent density of $18 \text{ uA} \cdot \text{cm}^{-2}$ at 1.23 V (vs. Ag/AgCl), which is even lower than the dark photocurrent of $30 \text{ uA} \cdot \text{cm}^{-2}$ at 1.23 V (vs. Ag/AgCl), indicating no photocurrent response of BiOCl as a photoanode.

The effect of HCl concentration on the PEC performance was also investigated to obtain the optimum condition for the preparation of BiVO₄/BiOCl heterojunction photoanode. As shown in Fig. 6, the sample treated with HCl concentration of 50 mM shows higher the photocurrent density than that of pristine BiVO₄, suggesting that the BiOCl layer is benefit for the photocurrent performance by forming BiVO₄/BiOCl heterojunction. With a higher HCl concentration of 75 mM, the highest photocurrent density was obtained, which could

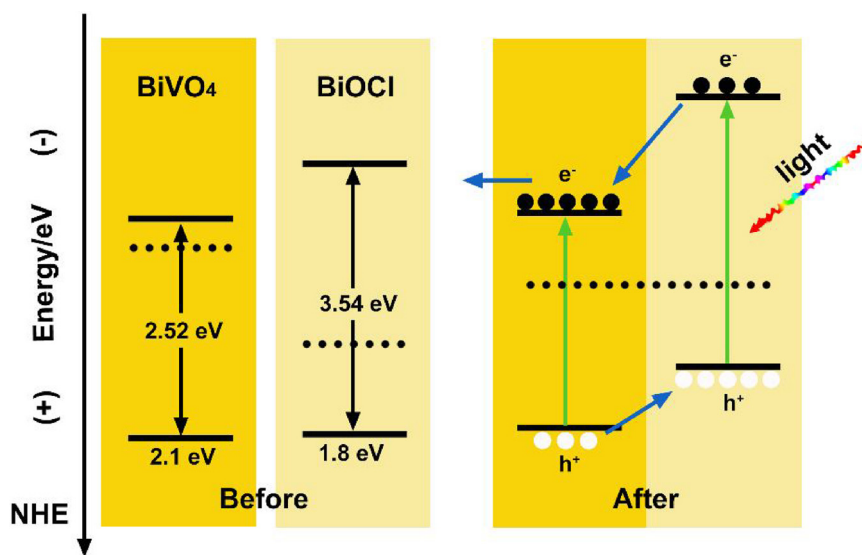


Fig. 10. Schematic band positions of the BiVO₄/BiOCl heterojunction before (left) and after (right) illumination.

due to forming BiVO₄/BiOCl heterojunction with proper thickness of BiOCl layer. Further increase of HCl concentration resulted in a significant decrease in photocurrent density, which could be ascribed to blocking of charge carrier transport by the BiOCl layer with excess thickness.

In order to gain a better insight into the photocurrent density enhancement, charge separation efficiency ($\eta_{\text{separation}}$) and injection efficiency ($\eta_{\text{injection}}$) tests were conducted in a 0.5 M Na₂SO₄ electrolyte containing 0.5 M H₂O₂ [29]. Generally, the obtained density ($J_{\text{H}_2\text{O}}$) can be expressed as the product of the rate of photon absorption (J_{absorbed}), $\eta_{\text{separation}}$ and $\eta_{\text{injection}}$, as the following equation:

$$J_{\text{H}_2\text{O}} = J_{\text{absorbed}} \times \eta_{\text{separation}} \times \eta_{\text{injection}} \quad (1)$$

Where the $\eta_{\text{separation}}$ and $\eta_{\text{injection}}$ refer to the fractions of photo-generated holes that survive from recombining with electrons in the bulk and those in surface traps, respectively. In the presence of H₂O₂, the $\eta_{\text{injection}}$ will be close to 100% ($\eta_{\text{injection}} = 1$) as the H₂O₂ plays a role as efficient hole scavenger in the electrolyte which avoid the recombination of photo-generated holes and electrons in surface traps [16,30]. Then the photocurrent density equation can be simplified as:

$$J_{\text{H}_2\text{O}_2} = J_{\text{absorbed}} \times \eta_{\text{separation}} \quad (2)$$

Thus, the $\eta_{\text{separation}}$ and $\eta_{\text{injection}}$ can be obtained simply by the following equations:

$$\eta_{\text{separation}} = J_{\text{H}_2\text{O}_2} / J_{\text{absorbed}} \quad (3)$$

$$\eta_{\text{injection}} = J_{\text{H}_2\text{O}} / J_{\text{H}_2\text{O}_2} \quad (4)$$

As shown in Fig. 7a, the charge separation efficiency of BiVO increased from 28% to 41% at 1.23 V (vs. Ag/AgCl) after surface HCl treatment with a formation of BiVO₄/BiOCl heterojunction indicates the heterojunction is benefit for the charge carriers extracting from BiVO₄ surface part. On the other hand, the injection efficiency of BiVO decreased from 80% to 75% at 1.23 V (vs. Ag/AgCl) after the same process (Fig. 7b) indicates the heterojunction is harm to the charge carriers transferring to electrolyte. By comparing both efficiencies with the photocurrent density result, one can conclude the benefit of heterojunction is better than the bad of heterojunction for the PEC performance.

To further explain the PEC performance enhancement and get a qualitative understanding of the charge transfer mechanism across BiVO₄/BiOCl interface, band positions of the samples were estimated according to their optical properties and ultraviolet photoelectron

spectroscopy (UPS) results instead of Mott-Schottky plots (Fig. S2). As a matter of fact, the band position of a semiconductor can be determined by its band gap and valance band potential (VB). The band gap can be extracted from the Uv-vis diffuse transmission spectra (DTS) curve [40] and the VB can be determined by extrapolating the x intercept of the linear portion of UPS plots [41,42].

Fig. 8 presents the DTS curves of as-prepared samples. A band gap of 2.52 eV (493 nm) and a band gap of 3.54 eV (350 nm) are recorded from the absorption thresholds of BiVO and BiOCl samples, respectively. Compared with the BiVO sample, the threshold of BiVO/BiOCl sample slightly blue shift to near 487 nm (corresponding to a band gap of 2.55 eV), indicating that the conversion of BiVO₄ to BiOCl layer at the surface increased the bandgap and resulted in lower photo utilization. Thus, the enhanced PEC response should attribute to other reasons rather photon absorption.

Fig. 9 presents the UPS results of as-prepared samples. The BiVO and BiOCl samples show VB levels of 2.1 eV and 1.8 eV, which are in accordance with the reported experimental data of 2.53 eV [43] and 2.40 eV [36], respectively. The BiVO/BiOCl heterojunction shows a VB level of 1.0 eV with a 0.8 eV negative shifting compared to BiOCl, indicating the heterojunction can shift the band position of BiVO/BiOCl surface part to negative direction under illumination.

In generally, the Fermi level (V_{fb}) is close to the conduction band for n-type semiconductor while close to the valence band for p-type semiconductor [41]. By considering the band gap and VB levels of the samples, one can draw the band-alignment diagram of the BiVO/BiOCl heterojunction, as shown in Fig. 10. Under illumination, electron-hole pairs generate in both BiVO₄ and BiOCl layers. The photogenerated electrons are apt to move from the conduction band (CB) of BiOCl layer to the CB of bulk BiVO₄ and further to the FTO substrate due to the formation of type II heterojunction. Meanwhile, the photogenerated holes can easily move from the VB of bulk BiVO₄ to the VB of BiOCl layer, follow with interfacial holes transfer and water oxidization. The significant PEC performance enhancement is therefore attributed to the effective charge separation with this type II band structure formed.

4. Conclusions

In summary, a BiVO₄/BiOCl heterojunction photoanode was fabricated for the first time by surface HCl treatment method. The formation process of BiVO₄/BiOCl heterojunction occurs through replacement of V—O bond to Cl—O covalent bond by Cl atoms attacking V atoms at the BiVO₄ surface. The formation of this heterojunction eliminates the

bismuth enrichment at the BiVO₄ surface, which is detrimental to its photocurrent response. Additionally, the BiVO₄/BiOCl heterojunction increased the photocurrent density of BiVO₄ from 1.27 mA/cm² to 1.83 mA/cm² at 1.23 V (vs. Ag/AgCl) as the formation of type II band alignment, which enhanced the charge separation efficiency of BiVO₄ from 28% to 41% at 1.23 V (vs. Ag/AgCl) in their interface. This paper demonstrate the conversion of surface elemental enrichment into a beneficial layer as an effective, simple approach to reduce surface recombination and improve the overall PEC performance for a solar energy conversion device.

Acknowledgements

We thank Dr. P.H. Guo for the XPS measurement, Dr. J. Wang for the TEM mapping measurement. We also gratefully thank the financial supports from the Fundamental Research Funds for the Central Universities (xjj2016039).

Appendix A. Supplementary data

Supplementary material related to this article can be found, in the online version, at doi:<https://doi.org/10.1016/j.apcatb.2018.09.060>.

References

- [1] D. Kang, T.W. Kim, S.R. Kubota, A.C. Cardiel, H.G. Cha, K.S. Choi, Chem. Rev. 115 (2015) 12839–12887.
- [2] N.K. Elumalai, A. Uddin, Energy Environ. Sci. 9 (2016) 391–410.
- [3] J. Su, L. Vayssières, ACS Energy Lett. 1 (2016) 121–135.
- [4] Y. Park, K.J. McDonald, K.S. Choi, Chem. Soc. Rev. 42 (2013) 2321–2337.
- [5] X. Shi, I.Y. Choi, K. Zhang, J. Kwon, D.Y. Kim, J.K. Lee, S.H. Oh, J.K. Kim, J.H. Park, Nat. Commun. 5 (2014) 4775.
- [6] C. Liu, X. Li, J. Su, L. Guo, Int. J. Hydrogen Energy 41 (2016) 12842–12851.
- [7] H.S. Han, S. Shin, D.H. Kim, I.J. Park, J.S. Kim, P.S. Huang, J.K. Lee, I.S. Cho, X.L. Zheng, Energy Environ. Sci. 11 (2018) 1299–1306.
- [8] J.K. Cooper, S. Gul, F.M. Toma, L. Chen, P.A. Glans, J. Guo, J.W. Ager, J. Yano, I.D. Sharp, Chem. Mater. 26 (2014) 5365–5373.
- [9] T. Das, X. Rocquefeite, R. Laskowski, L. Lajaunie, S. Jobic, P. Blaha, K. Schwarz, Chem. Mater. 29 (2017) 3380–3386.
- [10] F.F. Abdi, T.J. Savenije, M.M. May, B. Dam, R. van de Krol, J. Phys. Chem. Lett. 4 (2013) 2752–2757.
- [11] D.K. Lee, K.S. Choi, Nat. Energy 3 (2017) 53–60.
- [12] Z.F. Huang, L. Pan, J.J. Zou, X. Zhang, L. Wang, Nanoscale 6 (2014) 14044–14063.
- [13] T.S. Sinclair, B.M. Hunter, J.R. Winkler, H.B. Gray, A.M. Müller, Mater. Horiz. 2 (2015) 330–337.
- [14] Y.Y. Bu, J. Tian, Z.W. Chen, Q. Zhang, W.B. Li, F.H. Tian, J.P. Ao, Adv. Mater. Interfaces 4 (2017) 1601235.
- [15] F.F. Abdi, L. Han, A.H. Smets, M. Zeman, B. Dam, R. van de Krol, Nat. Commun. 4 (2013) 2195.
- [16] C. Liu, J.Z. Su, L.J. Guo, RSC Adv. 6 (2016) 27557–27565.
- [17] I. Grigioni, K.G. Stamplecoskie, D.H. Jara, M.V. Dozzi, A. Oriana, G. Cerullo, P.V. Kamat, E. Sell, ACS Energy Lett. 2 (2017) 1362–1367.
- [18] L. Xia, J. Bai, J. Li, Q. Zeng, X. Li, B. Zhou, Appl. Catal. B 183 (2016) 224–230.
- [19] H. Zhang, C. Cheng, ACS Energy Lett. 2 (2017) 813–821.
- [20] J. Su, C. Liu, D. Liu, M. Li, J. Zhou, ChemCatChem 8 (2016) 3279–3286.
- [21] T.W. Kim, K.S. Choi, Science 343 (2014) 990–994.
- [22] H. Yoon, M.G. Mai, J.Y. Choi, M.W. Kim, S.K. Choi, H. Park, S.S. Al-Deyab, M.T. Swihart, A.L. Yarin, S.S. Yoon, Langmuir 31 (2015) 3727–3737.
- [23] K.Y. Jang, G. Park, K.H. Oh, J.H. Seo, K.M. Nam, Chem. Commun. 53 (2017) 4120–4123.
- [24] Y. Wang, F. Li, X. Zhou, F. Yu, J. Du, L. Bai, L. Sun, Angew. Chem. Int. Ed. 56 (2017) 6911–6915.
- [25] Y.M. Ma, A. Kafizas, S.R. Pendlebury, F. Le Formal, J.R. Durrant, Adv. Funct. Mater. 26 (2016) 4951–4960.
- [26] C. Liu, J. Su, J. Zhou, L. Guo, ACS Sustain. Chem. Eng. 4 (2016) 4492–4497.
- [27] M.D. Rossell, P. Agrawal, A. Borgschulte, C. Hébert, D. Passerone, R. Erni, Chem. Mater. 27 (2015) 3593–3600.
- [28] S. Wang, P. Chen, J.H. Yun, Y. Hu, L.W. Wang, Angew. Chem. Int. Ed. 56 (2017) 8500–8504.
- [29] E.S. Kim, H.J. Kang, G. Magesh, J.Y. Kim, J.W. Jang, J.S. Lee, ACS Appl. Mat. Interfaces 6 (2014) 17762–17769.
- [30] J.H. Kim, Y.J. Jang, J.H. Kim, J.W. Jang, S.H. Choi, J.S. Lee, Nanoscale 7 (2015) 19144–19151.
- [31] K.H. Ye, Z. Chai, J. Gu, X. Yu, C. Zhao, Y. Zhang, W. Mai, Nano Energy 18 (2015) 222–231.
- [32] T.W. Kim, K.S. Choi, J. Phys. Chem. Lett. 7 (2016) 447–451.
- [33] W.Q. Fan, X.Q. Yu, S.Y. Song, H.Y. Bai, C. Zhang, D. Yan, C.B. Liu, Q. Wang, W.D. Shi, CrystEngComm 16 (2014) 820–825.
- [34] W.A. Smith, I.D. Sharp, N.C. Strandwitz, J. Bisquert, Energy Environ. Sci. 8 (2015) 2851–2862.
- [35] L. Chen, J. Yang, S. Klaus, L.J. Lee, R. Woods-Robinson, J. Ma, Y. Lum, J.K. Cooper, F.M. Toma, L.W. Wang, I.D. Sharp, A.T. Bell, J.W. Ager, J. Am. Chem. Soc. 137 (2015) 9595–9603.
- [36] Z. He, Y. Shi, C. Gao, L. Wen, J. Chen, S. Song, J. Phys. Chem. C 118 (2014) 389–398.
- [37] D.P. Jaihindh, Y.P. Fu, Catal. Today 297 (2017) 246–254.
- [38] L. Song, Y. Pan, Y. Zheng, C. Chen, L. Ge, J. Alloy Compd. 710 (2017) 375–382.
- [39] J. Jiang, K. Zhao, X. Xiao, L. Zhang, J. Am. Chem. Soc. 134 (2012) 4473–4476.
- [40] S. Byun, G. Jung, S.Y. Moon, B. Kim, J.Y. Park, S. Jeon, S.W. Nam, B. Shin, Nano Energy 43 (2018) 244–252.
- [41] S. Giménez, J. Bisquert, Photoelectrochemical Solar Fuel Production, Springer, Berlin, 2016.
- [42] W.J. Chun, A. Ishikawa, H. Fujisawa, T. Takata, J.N. Kondo, M. Hara, M. Kawai, Y. Matsumoto, K. Domen, J. Phys. Chem. B 107 (2003) 1798–1803.
- [43] S.J. Hong, S. Lee, J.S. Jang, J.S. Lee, Energy Environ. Sci. 4 (2011) 1781–1787.